Research Article

Journal of Chemical Research

Journal of Chemical Research
1–11

DOI: 10.1177/1747519820907248
journals.sagepub.com/home/chl
SAGE

Novel photosensitizing properties of porphyrin–chrysin derivatives with antitumor activity in vitro

Ding Liu[1,2], Qizhi Zhang[1,2], Lang Zhang[3], Wenmei Yu[1,2], Huizhi Long[1,2], Jun He[3] and Yunmei Liu[1,2]

Abstract

Photodynamic therapy is a promising cancer treatment with the advantages of low toxicity, high efficiency, and noninvasiveness. In this study, 23 novel porphyrin–chrysin derivatives are synthesized using alkyl carbon chains as bridges. We use human gastric cancer cells (MGC-803) and human cervical cancer cells to evaluate the in vitro antitumor activity of all the porphyrin–chrysin derivatives, with 5-fluorouracil (5-Fu) as a positive control. Several of the prepared compounds showed effective photodynamic killing effects, among which 5-hydroxy-2-phenyl-7-(2-(4-(10,15,20-tris(4-hydroxyphenyl)porphyrin-5-yl)phenoxy)ethoxy)-4*H*-chromen-4-one shows the highest antiproliferation activity on human cervical cancer cells, with a half maximal inhibitory concentration of 26.51 ± 1.15 μM. Flow cytometry analysis showed that human cervical cancer cell apoptosis might be induced by G1 phase arrest.

Keywords

porphyrins, chrysins, porphyrin-chrysin derivatives, synthesis, antitumor

Date received: 5 September 2019; accepted: 28 January 2020

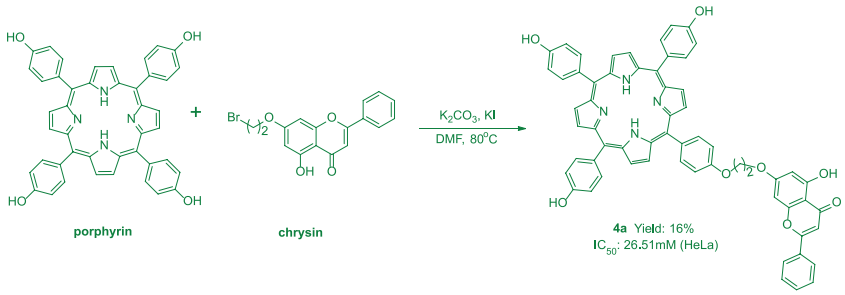

Introduction

Photodynamic therapy (PDT) is a new technology that was began to be applied to cancer therapy in the late 1970s. Thereafter, PDT has been accepted by the relevant departments of the United States, the United Kingdom, Germany, Japan, and other countries to enter clinical applications. Until now, this therapy has been used to treat a variety of malignancies successfully.[1–3]

The basic elements of PDT can be divided into photosensitizers, specific excitation light, and molecular oxygen. The photosensitizer transfers the absorbed energy to the surrounding oxygen molecules through light irradiation, so that the oxygen molecules become excited singlet oxygen ($^1O_2$) and other reactive oxygen species (ROS) to achieve the purpose of killing tumor cells.[4] In fact, the PDT beam is different from the usual clinical laser treatment in that its energy density is low, and its purpose is to activate the photosensitizer without causing tissue damage.

Although a number of photosensitizers have been suggested for PDT,[5] porphyrins, and their analogs remain the most extensively employed photosensitive compounds.[6,7] Porphyrins have the following advantages for PDT. On one hand, they are satisfactory for singlet oxygen production, and on the other hand, they have the ability to preferentially aggregate in tumor tissues. There are two general theories about the mechanism of specific aggregation of porphyrins in tumor tissues. According to pH theory, most porphyrin molecules enter the cell through

[1]Institute of Pharmacy & Pharmacology, Hunan Province Cooperative Innovation Center for Molecular Target New Drug Study, University of South China, Hengyang, P.R. China
[2]Hunan Provincial Key Laboratory of Tumor Microenvironment Responsive Drug Research, Hengyang, P.R. China
[3]Institute of Chemistry & Chemical Engineering, University of South China, Hengyang, P.R. China

Corresponding author:
Yunmei Liu, Institute of Pharmacy & Pharmacology, Hunan Province Cooperative Innovation Center for Molecular Target New Drug Study, University of South China, Hengyang 421001, P.R. China.
Email: lymhsm@126.com

passive diffusion. Numerous experiments have shown that porphyrin compounds are more conducive to maintaining the molecular state in a weakly acidic tumor cell environment compared to normal tissues, thereby facilitating their entry into tumor cells in molecular form.[8–10] Based on the theory of low-density lipoproteins (LDLs), the surface of rapidly growing tumor cells contains more LDL receptors that show strong activity. When the porphyrin compound binds to the LDLs, the LDLs transport the drug to bind to receptors on the cell membrane so that the drug can accumulate in the tumor tissue.[11–14] Based on this, a large number of antitumor porphyrin derivatives have been reported.[15–18]

Chrysin is a natural flavonoid and has a wide range of pharmacological activities such as anti-inflammatory,[19,20] antioxidant,[21,22] antibacterial,[23] hypoglycemic,[24] antitumor,[25–27] and so on. However, there are many shortcomings in the chemical structure of chrysin. Research by scientists in both China and abroad on chrysin has mainly focused on the modification and optimization of its chemical structure. On one hand, chrysin shows poor lipophilic and water-solubility properties, which limits its clinical application. Second, the 5- and 7-hydroxy groups of chrysin are readily inactivated by rapid glycosylation and metabolism in vivo. Therefore, the structural optimization of chrysin in order to improve its bioavailability and activity has been the subject of significant research.[28–30]

To this end, we have innovatively combined the antitumor compounds porphyrin and chrysin by appropriate methods. Finally, a series of novel porphyrin–chrysin derivatives have been obtained and the products tested for their performance and in vitro antitumor activity.

Results and discussion

Chemical synthesis

In this study, 23 novel substituted porphyrin–chrysin derivatives have been synthesized. First, we prepared the chrysin and porphyrin derivatives. The chrysin derivatives **1a–1e** were synthesized according to the method shown in Scheme 1, typically by alkylation of the chrysin 7-OH with 1, n-dihalogenated alkanes using KI or K_2CO_3, and the resulting compounds were consistent with the literature.[31,32] Porphyrins **2**–**4** were synthesized according to the classical Adler–Longo method shown in Scheme 2.[33–36] Metalloporphyrins **5** and **6** were obtained after metalizing porphyrins **2** and **3**.[37] The synthesis of the target compounds **2a**–**6e** followed the general pathway shown in Scheme 3. The porphyrins were dissolved in N,N-Dimethylformamide (DMF); potassium carbonate and potassium iodide were added; and the chrysin derivatives were added after reaction at 80°C for 1 h. The structures of all the target compounds were characterized by ^{1}H nuclear magnetic resonance (NMR), ultraviolet–visible spectroscopy (UV-Vis), and matrix-assisted laser desorption/ionization time-of-flight (MALDI-TOF) mass spectrometry (see the Supplemental material).

Performance testing

UV-Vis spectra. As shown in Table 1, the Soret band and the Q band are two characteristic absorption bands of the porphyrin compounds. The Soret band is generally around 418 nm and exhibits strong absorption. The Q band is generally between 500 and 700 nm and exhibits weak absorption. The II band is a characteristic absorption band of flavonoids.[38] We found that the Soret band absorption peaks of the derivatives **5** and **6** produced a slight blue shift, and the Q band absorption peaks decreased in intensity from **4** to **1** compared to derivatives **2** and **3**. This phenomenon can be explained by the fact that the insertion of nickel reduces the π-electron density of the porphyrin ring and makes the overall structure of the porphyrin molecule more symmetrical, increasing the degeneracy of the molecular orbital (see the Supplemental Material).

Fluorescence spectra. The results of fluorescence spectroscopy showed that the maximum fluorescence emission wavelengths of the derivatives **2**, **3**, and **4** were all around 656 nm, while no fluorescence signal was detected for

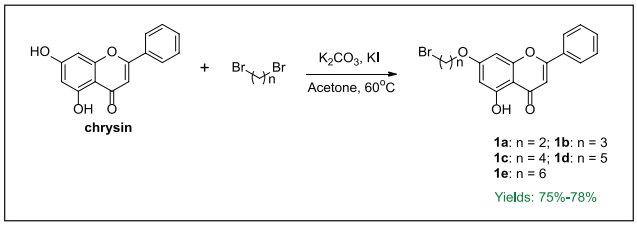

Scheme 1. Synthesis of the chrysin derivatives.

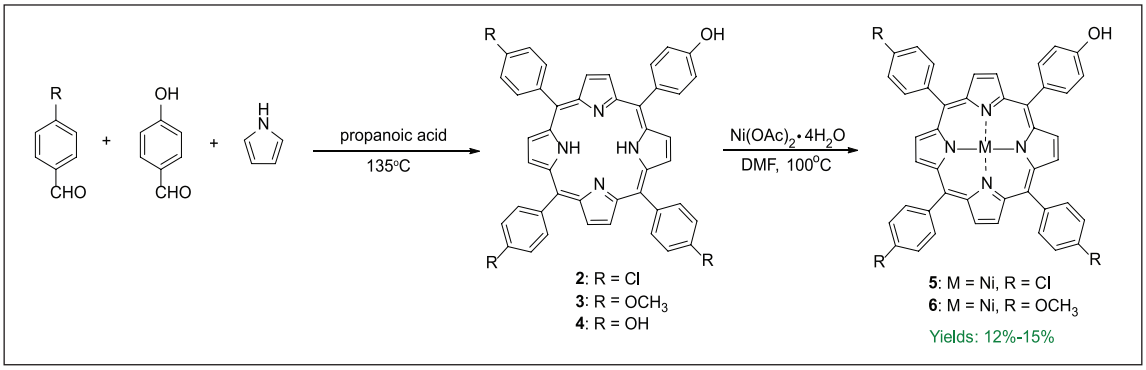

Scheme 2. Synthesis of the porphyrin compounds.

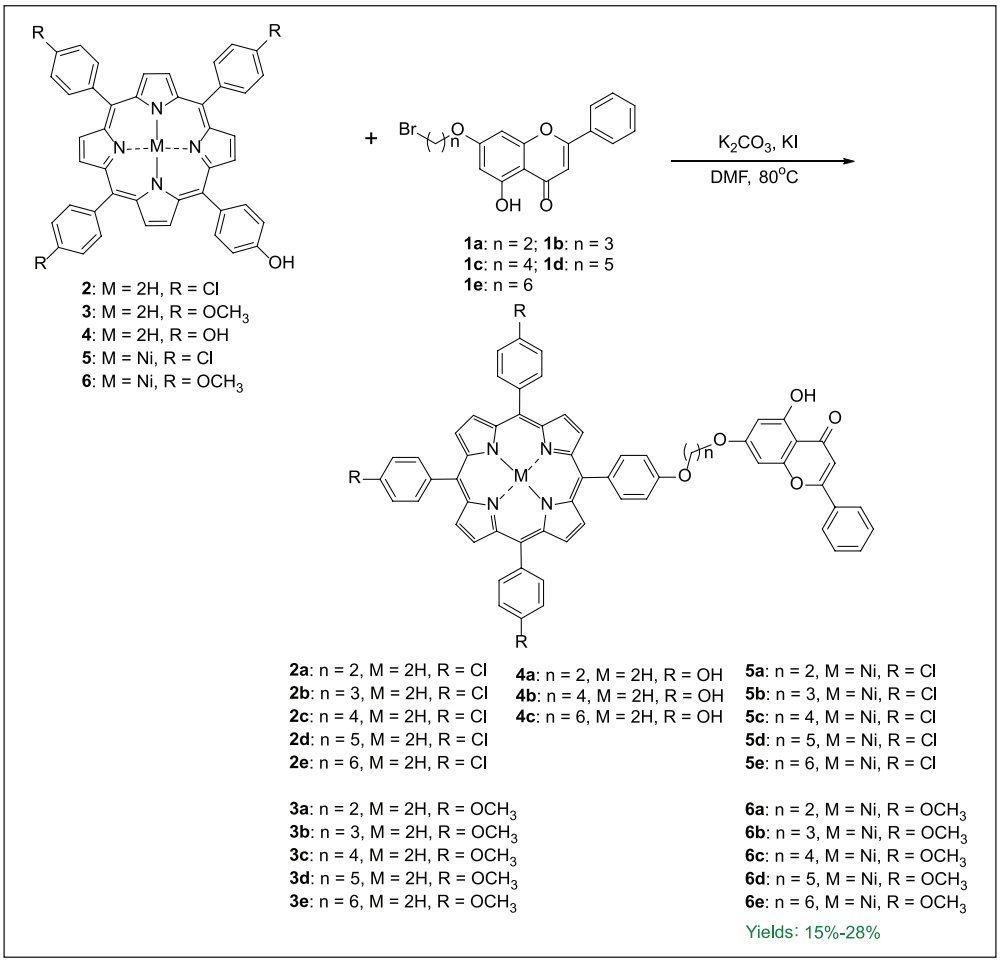

Scheme 3. Synthesis of the porphyrin–chrysin derivatives.

compounds **5** and **6**. Analysis has shown that there is a single electron in the d orbital of the extranuclear electron arrangement of the nickel atom. When the nickel atom is combined with the conjugated porphyrin molecule, this electron is still not paired, causing the entire conjugated structure to be destroyed, so the molecule dose not fluoresce[33] (see the Supplemental material).

Detection of singlet oxygen ($^1O_2$). $^1O_2$ is a powerful ROS, which can effectively induce the apoptosis of tumor cells. 1,3-Diphenylisobenzofuran (DPBF) is a commonly used singlet oxygen–trapping agent, which can be oxidized by singlet oxygen to open the ring and destroy the conjugated structure, resulting in the disappearance of the fluorescence signal. We have used the magnitude and rate of its fluorescence intensity change around 456 nm to evaluate the ability of compounds to produce singlet oxygen.[39] As shown in Figure 1, compared with the DPBF control group, the fluorescence intensity of the DPBF solution and the mixed solution of the target compounds porphyrin–chrysin derivatives **2a**–**6e** were decreased to varying degrees, which indicated that the porphyrin–chrysin derivatives had certain singlet oxygen production capacity.

Comparing the presence of Figure 1(b)–(d) with (e) and (f), it can be seen that the free-base porphyrin derivatives **2**, **3**, and **4** series have a stronger ability to generate singlet oxygen than the metalloporphyrins **5** and **6**. Within 10 min of monitoring, the DPBF fluorescence intensity of the porphyrin–chrysin derivatives **2**, **3**, and **4** was substantially reduced to below 200, while the DPBF fluorescence intensity of Derivatives **5** and **6** was generally between 500 and 800 counts.

Biological activities

In vitro antiproliferative activity assay. The antiproliferative activity in vitro of compounds **2**, **3**, **4**, **5**, **6**, **2a**–**2e**, **3a**–**3e**, **4a**–**4c**, **5a**–**5e**, and **6a**–**6e** were tested against human tumor cells: MGC-803 (gastric carcinoma cells) and HeLa (cervical carcinoma cells) using the 3-(4,5-dimethylthiazol-2-yl)-2,5-diphenyltetrazolium bromide (MTT) assay to determine the cytotoxicity of the compounds in light and darkness, respectively.[40] Some compounds exhibited moderate to good antiproliferative activity against the MGC-803 cell and HeLa cell lines.

According to the data in Table 2, the antiproliferative activity of the light group was significantly stronger than that of the dark group. Derivatives **2**, **3**, and **4** are more cytotoxic than **5** and **6**. Among derivatives **2**, **3**, and **4**, derivatives **4** had the best antitumor activity, followed by the derivatives **2**, with the compound **3** showing the worst activity. This phenomenon is almost consistent with the

Table 1. UV/Vis absorption spectral data of the porphyrin–chrysin derivatives.[a]

Compound	II band (nm)	Soret band (nm)	Q band (nm)
2	—	419	516, 552, 591, 647
2a	270	420	517, 552, 592, 647
2b	270	420	516, 552, 592, 647
2c	270	420	517, 552, 591, 647
2d	270	420	517, 552, 592, 648
2e	270	420	517, 552, 592, 647
5	—	416	529
5a	269	417	529
5b	269	417	529
5c	269	417	529
5d	269	417	529
5e	269	417	529
3	—	421	519, 556, 594, 649
3a	269	420	519, 556, 594, 649
3b	269	420	519, 556, 594, 649
3c	269	421	519, 556, 595, 649
3d	269	421	519, 556, 595, 650
3e	269	421	519, 556, 595, 650
6	—	419	530
6a	269	419	530
6b	269	419	530
6c	269	419	530
6d	269	419	530
6e	269	419	531
4	—	421	519, 556, 594, 650
4a	269	421	519, 556, 594, 650
4b	269	421	519, 556, 594, 650
4c	269	421	519, 556, 594, 650

[a]The structural formulae of the porphyrin–chrysin compounds are shown in Scheme 3.

ability of the compound to produce singlet oxygen. Compounds **2a**, **2c**, **2e**, **4a**, and **4b** have high antitumor activity under light conditions. The activity of **4a** compound on MGC-803 and HeLa cells was better than that of chrysin and the positive control drug 5-Fu, and its toxicity to HeLa cells was five times that compared to when in the dark.

Cell cycle assay. A cell cycle assay was conducted to check the distribution of HeLa cells, treated with compound **4a** at different concentrations (0, 20, 40, and 60 μM) over 24 h, in different phases under light conditions. As indicated in Figure 2, with the increase of drug concentration (0, 20, 40, and 60), the percentage of HeLa cells in the G1 phase gradually increased from 69.67% to 72.64%, 75.77%, and 78.85%. In contrast, the percentage of cells in the S and G2 phases gradually decreased. The results showed that compound **4a** inhibited HeLa cell proliferation in a concentration-dependent manner and blocked it in the G1 phase.

Apoptosis assay. The flow cytometry assay determined the effect of compound **4a** on apoptosis in HeLa cells. The cells were treated with compound **4a** at different concentrations (0, 20, 40, and 60 μM) under light conditions for 24 h and were collected, stained with Annexin V-fluorescein isothiocyanate (FITC)/PI, and then examined. In Figure 3, four-quadrant plots, the control group normal cells accounted for 82.6% of the total cell number, and apoptotic cells (Q2 + Q3) were only 15.53%, when the drug concentration was increased to 60 μM, normal cells accounted for only 10.3%, and the number of apoptotic cells increased to 88.58%. Therefore, we can conclude that compound **4a** can induce apoptosis in HeLa cells in a concentration-dependent manner.

Conclusion

In summary, a series of novel porphyrin–chrysin derivatives have been synthesized, and these compounds were evaluated for their $^1O_2$ and antitumor activities. The results of MTT in vitro antiproliferative experiments showed that compounds **2a**, **2c**, **2e**, **4a**, and **4b** had higher antiproliferative activity against MGC-803 and HeLa cells under light conditions. Compound **4a** had significant inhibitory activity against HeLa cells under light conditions, with the IC_{50} value (26.51 ± 1.15) being much lower than that of the positive control drug 5-Fu. At the same time, the activity of the free-base porphyrin derivatives is higher than that of the nickel porphyrin derivatives. In addition, the antiproliferative effect of all compounds was significantly enhanced under light conditions compared to dark conditions.

Experimental section

All the starting materials, solvents, and reagents were reagent grade and purchased from commercial sources unless otherwise stated. Chrysin was purchased from Aladdin. ^{1}H NMR was recorded on a Bruker AVANCE instrument (400 and 500 MHz, Bruker, Germany). MALDI-TOF MS data were recorded using a Bruker Daltonics flex analyzer (Bruker, Germany).

Synthesis methods

Synthesis of chrysin derivatives **1a–1e.**[31,32]. The appropriate 1, n-dibromoalkane (10 mmol), K_2CO_3 (50 mmol), and KI (50 mmol) were dissolved in acetone (60 mL) and stirred at 60°C for 1 h under reflux. Next, chrysin (508.5 mg, 2 mmol) was slowly added to the reaction system in batches, and the reaction progress was monitored by thin-layer chromatography (TLC) until the reaction was complete. The reaction solution was extracted with dichloromethane and washed twice with water to remove impurities. The organic layer was dried over anhydrous Na_2SO_4, and then the solvent was distilled off under reduced pressure. The residue purified by silica gel column chromatography. The first color band was collected with dichloromethane/*n*-hexane (3: 1) as eluent, and yellow crystals were obtained by recrystallization from *n*-hexane.

Synthesis of porphyrin compounds **2**, **3**, *and* **4.**[33–36]. Compounds **2** or **3** were prepared using (6.2 g, 0.05 mol) *p*-hydroxybenzaldehyde and *p*-chlorobenzaldehyde (14.0 g,

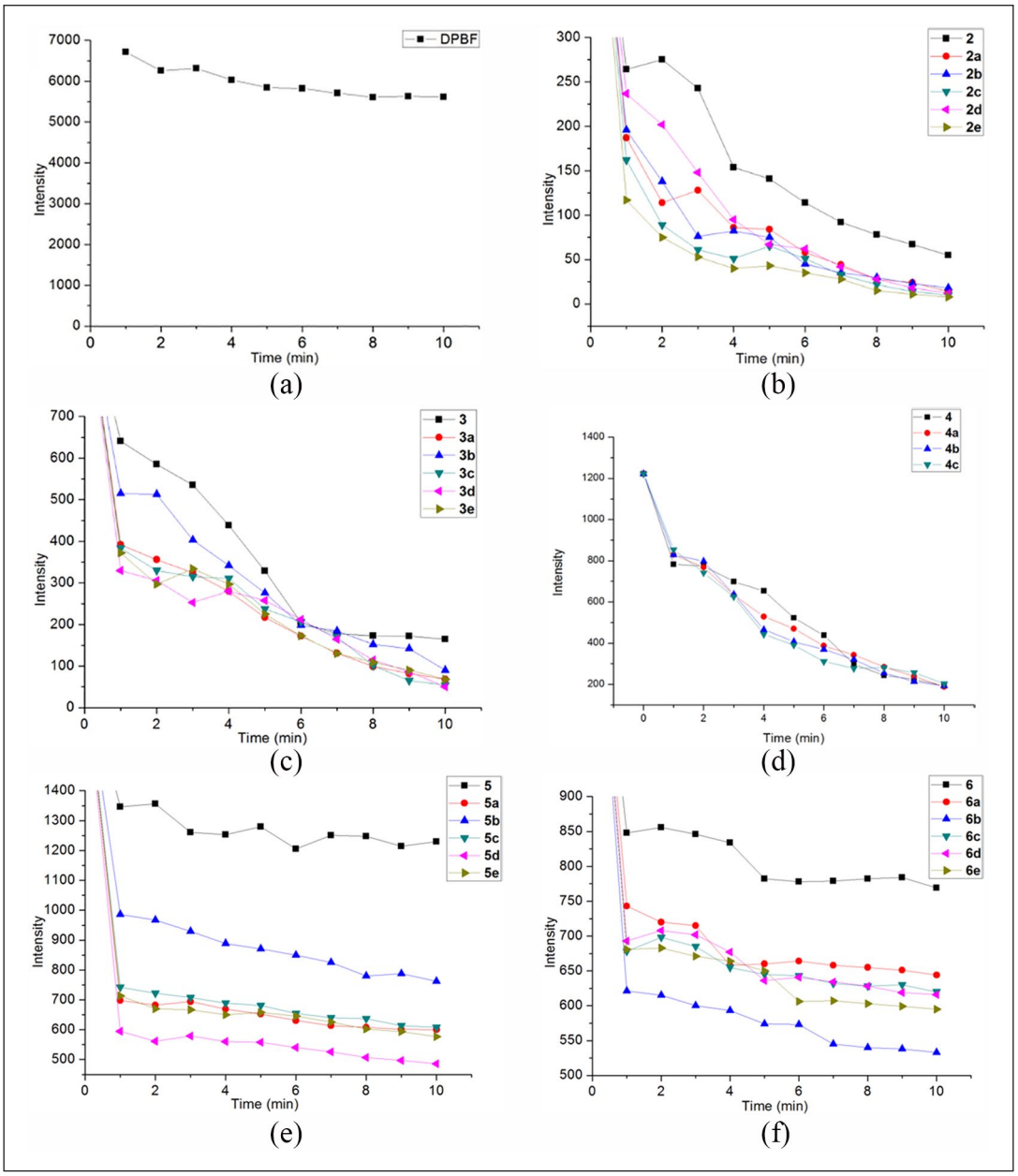

Figure 1. Singlet oxygen yields of the porphyrin–chrysin derivatives and DPBF (a) is the change of fluorescence intensity of DPBF within 10 min; (b)–(f), are the changes of the fluorescence intensities of DPBF within 10 min, respectively, in the derivatives **2**, **3**, **4**, **5**, and **6**.

0.10 mol) or *p*-methoxybenzaldehyde (13.6 g, 0.10 mol). For compound **4**, only of *p*-hydroxybenzaldehyde (12.4 g, 0.10 mol) was added. Next, propionic acid (200 mL) was added, and the mixture was stirred at 135°C under reflux, and Freshly distilled pyrrole (10.2 g, 0.15 mol) was slowly added dropwise to the reaction solution over 30 min using a constant pressure dropping funnel. After heating and refluxing for 1 h, the reaction was terminated by distilling off two-thirds of the propionic acid under reduced pressure, and an equivalent amount of anhydrous ethanol was added to the reaction solution. The mixture was allowed to stand at 4°C for 24 h, and then filtered under reduced pressure. The residue was washed several times with anhydrous ethanol. The residual solids were purified by silica gel and eluting with dichloromethane to obtain the corresponding porphyrins as purple crystals.

Synthesis of nickel metalloporphyrin compounds **5** *and* **6.**[37]. Porphyrin **2** (220.2 mg, 0.3 mmol) or **3** (218.4 mg, 0.3 mmol) and a five-fold equivalent amount nickel(II) acetate tetrahydrate were dissolved in DMF (80 mL) and the mixture heated at reflux with stirring. The reaction progress was monitored by TLC. After cooling, the reaction solution was extracted with dichloromethane and washed with water several times to remove excess nickel(II) acetate tetrahydrate. The organic layer was dried over anhydrous Na_2SO_4, the solvent distilled off under reduced pressure, and the obtained crystals recrystallized from anhydrous ethanol to give red-brown crystalline compounds **5** and **6**. Compound **5** has not been reported in the literature.

Synthesis of porphyrin–chrysin derivatives **2a–e**, **3a–e**, **4a–c**, **5a–e**, *and* **6a–e**. Compound **2** (110.1 mg), **3** (118.1 mg), **5**

Table 2. Anti-proliferative activity against tumor cell lines.

Compound	IC_{50} (μM)			
	MGC-803		HeLa	
	Light	Dark	Light	Dark
Chrysin	143.4 ± 4.76		>200	
2	148.5 ± 5.08	>200	>200	>200
2a	98.63 ± 3.26	>200	149.8 ± 4.17	>200
2b	>200	>200	>200	N.D
2c	85.75 ± 3.03	>200	131.6 ± 4.24	>200
2d	>200	N.D	166.5 ± 4.11	N.D
2e	81.87 ± 2.87	>200	>200	N.D
5	144.5 ± 3.75	N.D	167.7 ± 3.42	>200
5a	>200	N.D	132.9 ± 4.79	>200
5b	115.2 ± 4.60	>200	N.D	N.D
5c	>200	N.D	N.D	N.D
5d	147.4 ± 3.96	N.D	N.D	N.D
5e	171.6 ± 5.60	N.D	>200	N.D
3	>200	>200	>200	N.D
3a	>200	>200	179.1 ± 4.36	N.D
3b	>200	N.D	>200	N.D
3c	178.7 ± 5.13	>200	>200	N.D
3d	>200	N.D	N.D	N.D
3e	>200	N.D	>200	N.D
6	N.D	N.D	>200	N.D
6a	>200	N.D	>200	N.D
6b	>200	N.D	N.D	N.D
6c	N.D	N.D	N.D	N.D
6d	N.D	N.D	>200	N.D
6e	N.D	N.D	N.D	N.D
4	159.2 ± 3.43	>200	194.7 ± 3.07	>200
4a	70.41 ± 2.15	135.2 ± 2.42	26.51 ± 1.15	142.7 ± 2.45
4b	164.3 ± 5.33	>200	62.79 ± 2.22	170.3 ± 3.25
4c	>200	N.D	>200	N.D
5-Fu	78.37 ± 2.47		72.80 ± 2.27	

ND = not detected.

(118.5 mg), **6** (116.6 mg) (0.15 mmol) was dissolved in DMF (40 mL), and potassium iodide and potassium carbonate were added as acid binding agents, and reacted at 80°C for 30 minutes, and then chrysin derivative **1a–e** (0.18 mmol) was added, the temperature remained constant, and the reaction progress was monitored by TLC until complete. The reaction solution was extracted with dichloromethane and washed with water several times to remove impurities such as potassium carbonate and potassium iodide. After drying and concentration, the residue it was purified by silica gel column chromatography (dichloromethane/*n*-hexane, 3:1) then purified again by gel permeation chromatography and recrystallized from anhydrous ethanol to give red-purple crystalline compounds **2a–e**, **3a–e**, **5a–e**, and **6a–e**. Because compounds **4** are susceptible to multiple substitution reactions, they were prepared using a slightly different method. In order to obtain the target compounds and minimize the production of multiple substitution products (difficult to separate), the chrysin derivatives needed to be slowly added to the reaction system in batches. After the reaction was complete, the product was purified by silica gel column chromatography (dichloromethane/ethanol, 12:1). The third color band was collected, then purified again by gel permeation chromatography, and recrystallized from anhydrous ethanol to give red-purple crystals. In fact, small amounts of di- and tri-substituted products were formed but were difficult to separate, so they were not isolated.

5-Hydroxy-2-phenyl-7-(2-(4-(10,15,20-tris(4-chlorophenyl)porphyrin-5-yl)phenoxy)ethoxy)-4*H*-chromen-4-one (2a) Yield 15%. ^{1}H NMR (400 MHz, $CDCl_3$): δ = 12.80 (s, 1H), 8.90 (d, *J* = 4.7 Hz, 2H), 8.84 (s, 6H), 8.14 (t, *J* = 8.2 Hz, 8H), 7.91 (d, *J* = 7.0 Hz, 2H), 7.75 (d, *J* = 8.2 Hz, 6H), 7.59−7.50 (m, 3H), 7.34 (d, *J* = 8.3 Hz, 2H), 6.71 (s, 1H), 6.68 (s, 1H), 6.55 (s, 1H), 4.65 (s, 2H), 4.60 (s, 2H), −2.83 (s, 2H); UV/Vis ($CHCl_3$): λ_{max} = 270 nm (II band); 420 nm (Soret band); 517, 552, 592, 647 nm (Q bands); Fluorescence ($CHCl_3$): λ_{ex} = 417 nm, λ_{em} = 656 nm; MS (MALDI-TOF): *m/z* calcd for $C_{61}H_{39}Cl_3N_4O_5^+$ 1012.20 $[M + H]^+$, found 1012.12.

5-Hydroxy-2-phenyl-7-(3-(4-(10,15,20-tris(4-chlorophenyl)porphyrin-5-yl)phenoxy)propoxy)-4*H*-chromen-4-one (2b) Yield 17%. ^{1}H NMR (500 MHz, $CDCl_3$): δ = 12.76 (s, 1H), 8.89 (d, *J* = 4.2 Hz, 2H),

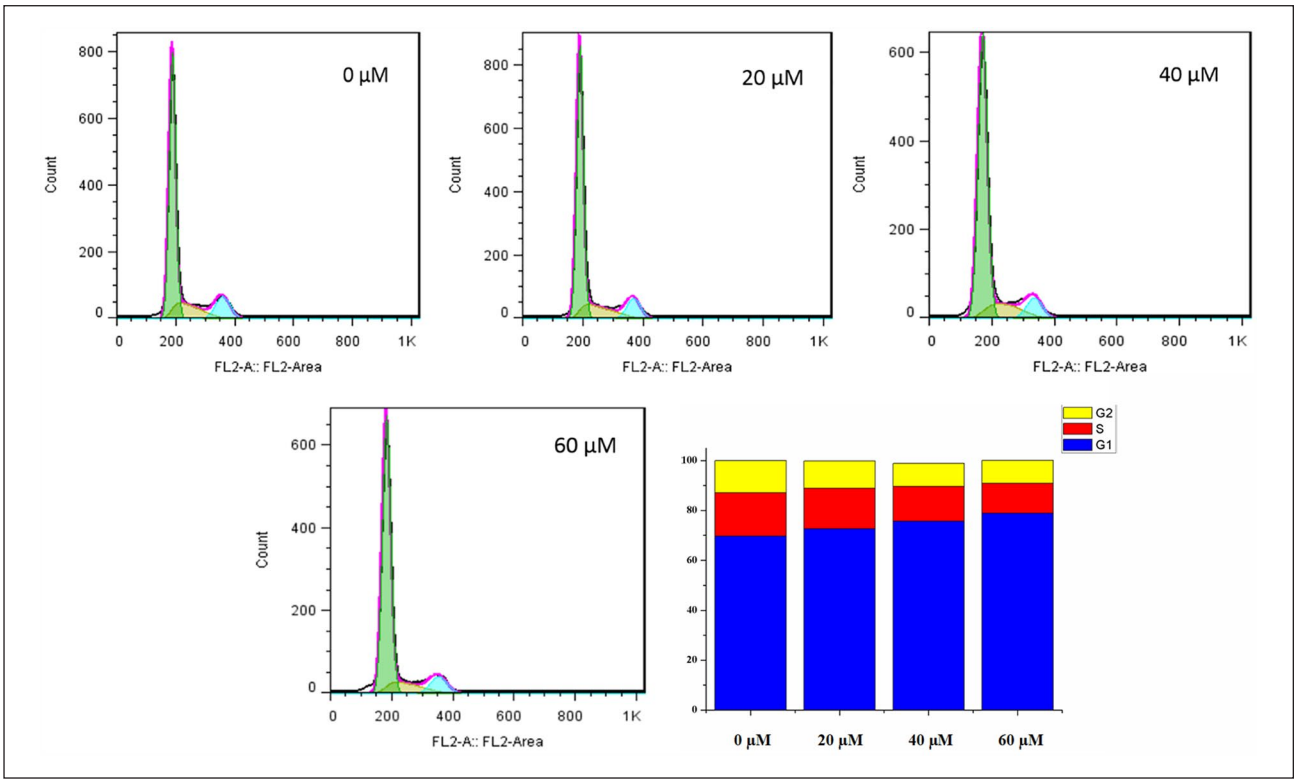

Figure 2. Inhibition of the cell cycle of HeLa cells by compound **4a**.

8.86−8.75 (m, 6H), 8.12 (t, J=8.5 Hz, 8H), 7.91 (d, J=6.5 Hz, 2H), 7.74 (d, J=7.1 Hz, 6H), 7.53 (d, J=7.1 Hz, 3H), 7.31 (d, J=8.2 Hz, 2H), 6.69 (s, 1H), 6.64 (s, 1H), 6.50 (s, 1H), 4.47 (t, J=5.7 Hz, 2H), 4.43 (t, J=5.9 Hz, 2H), 2.55−2.45 (m, 2H), −2.83 (s, 2H); UV/Vis ($CHCl_3$): λ_{max}=270 nm (II band); 420 nm (Soret band); 516, 552, 592, and 647 nm (Q bands); fluorescence ($CHCl_3$): λ_{ex}=417 nm, λ_{em}=656 nm; MS (MALDI-TOF): *m/z* calcd for $C_{62}H_{41}Cl_3N_4O_5^+$ 1026.21 $[M+H]^+$, found 1026.13.

5-Hydroxy-2-phenyl-7-(4-(4-(10,15,20-tris(4-chlorophenyl)porphyrin-5-yl)phenoxy)butoxy)-4*H*-chromen-4-one (2c) Yield 18%. ^{1}H NMR (500 MHz, $CDCl_3$): δ=12.76 (s, 1H), 8.91 (s, 2H), 8.83(s, 6H), 8.13 (t, J=8.6 Hz, 8H), 7.89 (d, J=7.2 Hz, 2H), 7.74 (d, J=7.9 Hz, 6H), 7.50 (t, J=7.5 Hz, 3H), 7.30 (d, J=7.9 Hz, 2H), 6.69 (s, 1H), 6.59 (s, 1H), 6.46 (s, 1H), 4.36 (s, 2H), 4.26 (s, 2H), 2.21 (s, 4H), −2.84 (s, 2H); UV/Vis ($CHCl_3$): λ_{max}=270 nm (II band); 420 nm (Soret band); 517, 552, 591, and 647 nm (Q bands); fluorescence ($CHCl_3$): λ_{ex}=417 nm, λ_{em}=656 nm; MS (MALDI-TOF): *m/z* calcd for $C_{63}H_{43}Cl_3N_4O_5^+$ 1040.23 $[M+H]^+$, found 1040.15.

5-Hydroxy-2-phenyl-7-((5-(4-(10,15,20-tris(4-chlorophenyl)porphyrin-5-yl)phenoxy)pentyl)oxy)-4*H*-chromen-4-one (2d) Yield 25%. ^{1}H NMR (500 MHz, $CDCl_3$): δ=12.75 (s, 1H), 8.91 (d, J=4.2 Hz, 2H), 8.83 (s, 6H), 8.12 (dd, J=13.4, 8.3 Hz, 8H), 7.86 (d, J=6.7 Hz, 2H), 7.74 (d, J=8.0 Hz, 6H), 7.50 (dt, J=14.2, 7.5 Hz, 3H), 7.29 (d, J=8.4 Hz, 2H), 6.65 (s, 1H), 6.56 (d, J=2.0 Hz, 1H), 6.44 (d, J=2.0 Hz, 1H), 4.30 (t, J=6.1 Hz, 2H), 4.17 (t, J=6.3 Hz, 2H), 2.14−1.97 (m, 4H), 1.86 (dd, J=15.0, 8.0 Hz, 2H), −2.84 (s, 2H); UV/Vis ($CHCl_3$): λ_{max}=270 nm (II band); 420 nm (Soret band); 517, 552, 591, and 648 nm (Q bands); fluorescence ($CHCl_3$): λ_{ex}=417 nm, λ_{em}=656 nm; MS (MALDI-TOF): *m/z* calcd for $C_{64}H_{45}Cl_3N_4O_5^+$ 1054.25 $[M+H]^+$, found 1054.16.

5-Hydroxy-2-phenyl-7-((6-(4-(10,15,20-tris(4-chlorophenyl)porphyrin-5-yl)phenoxy)hexyl)oxy)-4*H*-chromen-4-one (2e) Yield 26%. ^{1}H NMR (500 MHz, $CDCl_3$): δ=12.76 (s, 1H), 8.94 (d, J=4.7 Hz, 2H), 8.86 (d, J=5.7 Hz, 6H), 8.15 (t, J=7.3 Hz, 8H), 7.88 (d, J=7.3 Hz, 2H), 7.77 (d, J=7.8 Hz, 6H), 7.51 (d, J=7.9 Hz, 3H), 7.31 (d, J=8.0 Hz, 2H), 6.67 (s, 1H), 6.57 (d, J=2.2 Hz, 1H), 6.45 (d, J=2.2 Hz, 1H), 4.30 (t, J=6.3 Hz, 2H), 4.15 (t, J=6.4 Hz, 2H), 2.09−1.98 (m, 4H), 1.80−1.71 (m, 4H), −2.81 (s, 2H); UV/Vis ($CHCl_3$): λ_{max}=270 nm (II band); 420 nm (Soret band); 517, 552, 592, 647 nm (Q bands); fluorescence ($CHCl_3$): λ_{ex}=417 nm, λ_{em}=656 nm; MS (MALDI-TOF): *m/z* calcd for $C_{65}H_{47}Cl_3N_4O_5^+$ 1068.26 $[M+H]^+$, found 1068.19.

5-Hydroxy-2-phenyl-7-(2-(4-(10,15,20-tris(4-methoxyphenyl)porphyrin-5-yl)phenoxy)ethoxy)-4*H*-chromen-4-one (3a) Yield 17%. ^{1}H NMR (500 MHz, $CDCl_3$): δ=12.79 (s, 1H), 8.97−8.69 (m, 8H), 8.12 (d, J=8.3 Hz, 8H), 7.92 (d, J=6.5 Hz, 2H), 7.57−7.50 (m, 3H), 7.28 (d, J=8.4 Hz, 8H), 6.71 (s, 1H), 6.65 (d, J=1.7 Hz, 1H), 6.53 (s, 1H), 4.53 (s, 4H), 4.09 (s, 9H), −2.73 (s, 2H); UV/Vis ($CHCl_3$): λ_{max}=269 nm (II band); 420 nm (Soret band); 519, 556, 594, and 649 nm (Q bands); fluorescence ($CHCl_3$): λ_{ex}=417 nm, λ_{em}=656 nm; MS (MALDI-TOF): *m/z* calcd for $C_{64}H_{48}N_4O_8^+$ 1000.35 $[M+H]^+$, found 1000.31.

5-Hydroxy-2-phenyl-7-(3-(4-(10,15,20-tris(4-methoxyphenyl)porphyrin-5-yl)phenoxy)propoxy)-4*H*-chromen-4-one (3b) Yield 17%. ^{1}H NMR (500 MHz,

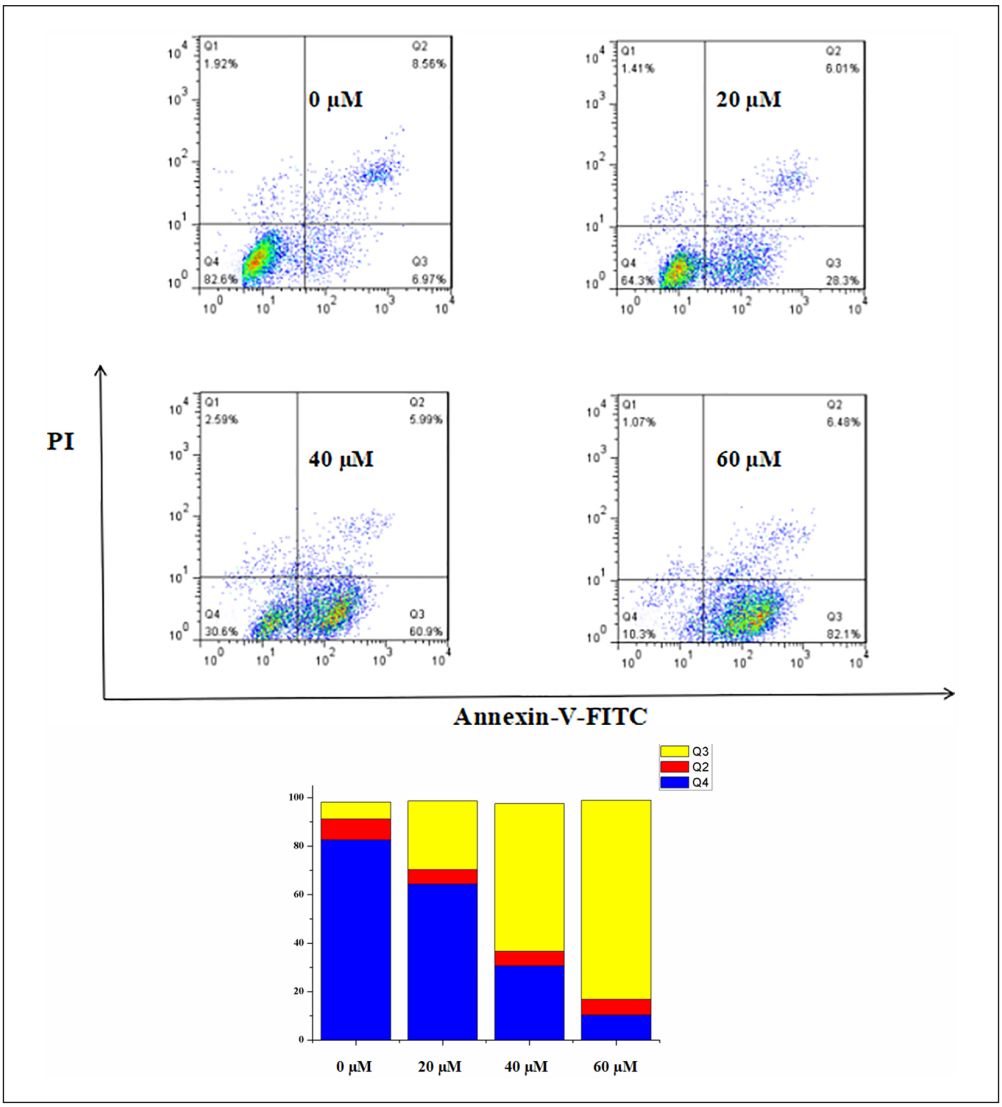

Figure 3. Effect of compound **4a** on apoptosis of HeLa cells. The Q1 region represents the number of mechanically injured cells, Q2 represents the late apoptotic cells, Q3 represents the early apoptotic cells, and Q4 represents the normal cells.

$CDCl_3$): δ = 12.76 (s, 1H), 8.86 (d, *J* = 5.3 Hz, 8H), 8.12 (d, *J* = 7.2 Hz, 8H), 7.91 (dd, *J* = 7.5, 1.6 Hz, 2H), 7.52 (d, *J* = 6.9 Hz, 3H), 7.29 (t, *J* = 7.2 Hz, 8H), 6.70 (s, 1H), 6.65 (d, *J* = 2.0 Hz, 1H), 6.51 (d, *J* = 2.0 Hz, 1H), 4.60 − 4.34 (m, 4H), 4.10 (s, 9H), 2.69 − 2.26 (m, 2H), −2.75 (s, 2H); UV/Vis ($CHCl_3$): λ_{max} = 269 nm (II band); 420 nm (Soret band); 519, 556, 594, and 649 nm (Q bands); fluorescence ($CHCl_3$): λ_{ex} = 417 nm, λ_{em} = 656 nm; MS (MALDI-TOF): *m/z* calcd for $C_{65}H_{50}N_4O_8^+$ 1014.36 $[M + H]^+$, found 1014.31.

5-Hydroxy-2-phenyl-7-(4-(4-(10,15,20-tris(4-methoxyphenyl)porphyrin-5-yl)phenoxy)butoxy)-4*H*-chromen-4-one (3c) Yield 23%. ^{1}H NMR (500 MHz, $CDCl_3$): δ = 12.77 (s, 1H), 8.87 (s, 8H), 8.12 (d, *J* = 8.3 Hz, 8H), 7.91 − 7.76 (m, 2H), 7.57 − 7.41 (m, 3H), 7.28 (d, *J* = 8.4 Hz, 8H), 6.68 (s, 1H), 6.59 (d, *J* = 2.0 Hz, 1H), 6.46 (d, *J* = 2.1 Hz, 1H), 4.32 (s, 2H), 4.24 (d, *J* = 5.2 Hz, 2H), 4.09 (s, 9H), 2.19 (s, 4H), −2.75 (s, 2H); UV/Vis ($CHCl_3$): λ_{max} = 269 nm (II band); 421 nm (Soret band); 519, 556, 595, and 649 nm (Q bands); fluorescence ($CHCl_3$): λ_{ex} = 417 nm, λ_{em} = 656 nm; MS (MALDI-TOF): *m/z* calcd for $C_{66}H_{52}N_4O_8^+$ 1028.38 $[M + H]^+$, found 1028.34.

5-Hydroxy-2-phenyl-7-((5-(4-(10,15,20-tris(4-methoxyphenyl)porphyrin-5-yl)phenoxy)pentyl)oxy)-4*H*-chromen-4-one (3d) Yield 28%. ^{1}H NMR (500 MHz, $CDCl_3$): δ = 12.74 (s, 1H), 8.86 (s, 8H), 8.12 (d, *J* = 8.0 Hz, 8H), 7.87 (d, *J* = 6.6 Hz, 2H), 7.49 (t, *J* = 7.4 Hz, 3H), 7.29 (d, *J* = 8.3 Hz, 8H), 6.66 (s, 1H), 6.57 (d, *J* = 2.0 Hz, 1H), 6.44 (d, *J* = 1.9 Hz, 1H), 4.30 (t, *J* = 6.1 Hz, 2H), 4.17 (t, *J* = 6.3 Hz, 2H), 4.10 (s, 9H), 2.13 − 1.98 (m, 4H), 1.91 − 1.78 (m, 2H), −2.75 (s, 2H); UV/Vis ($CHCl_3$): λ_{max} = 269 nm (II band); 421 nm (Soret band); 519, 556, 595, and 650 nm (Q bands); fluorescence ($CHCl_3$): λ_{ex} = 417 nm, λ_{em} = 656 nm; MS (MALDI-TOF): *m/z* calcd for $C_{67}H_{54}N_4O_8^+$ 1042.39 $[M + H]^+$, found 1042.35.

5-Hydroxy-2-phenyl-7-((6-(4-(10,15,20-tris(4-methoxyphenyl)porphyrin-5-yl)phenoxy)hexyl)oxy)-4*H*-chromen-4-one (3e) Yield 28%. ^{1}H NMR (500 MHz, $CDCl_3$): δ = 12.75 (s, 1H), 8.88 (s, 8H), 8.12 (t, *J* = 7.6 Hz, 8H), 7.86 (d, *J* = 6.7 Hz, 2H), 7.47 (d, *J* = 7.2 Hz, 3H), 7.28 (d, *J* = 8.3 Hz, 8H), 6.66 (s, 1H), 6.55 (s, 1H), 6.43 (s, 1H), 4.24 (t, *J* = 6.2 Hz, 2H), 4.12 (t, *J* = 6.4 Hz, 2H), 4.08 (s, 9H), 2.04 − 1.99 (m, 2H), 1.98 − 1.90 (m, 2H), 1.75 − 1.64 (m,

4H), −2.74 (s, 2H); UV/Vis ($CHCl_3$): λ_{max}=269 nm (II band); 421 nm (Soret band); 519, 556, 595, and 650 nm (Q bands); fluorescence ($CHCl_3$): λ_{ex}=417 nm, λ_{em}=656 nm; MS (MALDI-TOF): *m/z* calcd for $C_{68}H_{56}N_4O_8^+$ 1056.41 $[M+H]^+$, found 1056.38.

5-Hydroxy-2-phenyl-7-(2-(4-(10,15,20-tris(4-hydroxyphenyl)porphyrin-5-yl)phenoxy)ethoxy)-4*H*-chromen-4-one (4a) Yield 16%. ^{1}H NMR (500 MHz, DMSO-d_6): δ=12.88 (s, 1H), 9.98 (s, 3H), 8.86 (d, *J*=11.9 Hz, 8H), 8.14 (d, *J*=6.3 Hz, 4H), 8.00 (d, *J*=7.9 Hz, 6H), 7.71−7.56 (m, 3H), 7.43 (d, *J*=8.2 Hz, 2H), 7.21 (d, *J*=8.1 Hz, 6H), 7.10 (s, 1H), 7.02 (s, 1H), 6.59 (s, 1H), 4.65 (t, *J*=6.2 Hz, 2H), 4.56 (t, *J*=6.2 Hz, 2H), −2.90 (s, 2H); UV/Vis ($CHCl_3$): λ_{max}=269 nm (II band); 421 nm (Soret band); 519, 556, 594, and 650 nm (Q bands); fluorescence ($CHCl_3$): λ_{ex}=417 nm, λ_{em}=656 nm; MS (MALDI-TOF): *m/z* calcd for $C_{61}H_{42}N_4O_8^+$ 958.30 $[M+H]^+$, found 958.17.

5-Hydroxy-2-phenyl-7-(4-(4-(10,15,20-tris(4-hydroxyphenyl)porphyrin-5-yl)phenoxy)butoxy)-4*H*-chromen-4-one (4b) Yield 16%. ^{1}H NMR (500 MHz, DMSO-d_6): δ=12.81 (s, 1H), 9.95 (s, 3H), 8.87 (d, *J*=5.7 Hz, 6H), 8.83 (s, 2H), 8.08 (dd, *J*=14.7, 7.8 Hz, 4H), 8.01−7.94 (m, 6H), 7.54 (dt, *J*=15.1, 7.2 Hz, 3H), 7.35 (d, *J*=8.2 Hz, 2H), 7.21 (d, *J*=8.0 Hz, 6H), 6.99 (d, *J*=14.4 Hz, 1H), 6.86 (d, *J*=2.3 Hz, 1H), 6.46 (d, *J*=2.1 Hz, 1H), 4.32−4.20 (m, 4H), 2.04 (s, 4H), −2.88 (s, 2H); UV/Vis ($CHCl_3$): λ_{max}=269 nm (II band); 421 nm (Soret band); 519, 556, 594, and 650 nm (Q bands); fluorescence ($CHCl_3$): λ_{ex}=417 nm, λ_{em}=656 nm; MS (MALDI-TOF): *m/z* calcd for $C_{63}H_{46}N_4O_8^+$ 986.33 $[M+H]^+$, found 986.21.

5-Hydroxy-2-phenyl-7-((6-(4-(10,15,20-tris(4-hydroxyphenyl)porphyrin-5-yl)phenoxy)hexyl)oxy)-4*H*-chromen-4-one (4c) Yield 18%. ^{1}H NMR (500 MHz, DMSO-d_6): δ=12.81 (s, 1H), 9.98 (s, 3H), 8.87 (s, 6H), 8.83 (s, 2H), 8.09 (d, *J*=8.2 Hz, 2H), 8.05 (d, *J*=7.5 Hz, 2H), 8.02−7.98 (m, 6H), 7.59−7.48 (m, 3H), 7.35 (d, *J*=8.3 Hz, 2H), 7.20 (d, *J*=8.1 Hz, 6H), 7.00 (s, 1H), 6.86 (s, 1H), 6.43 (s, 1H), 4.26 (t, *J*=6.1 Hz, 2H), 4.17 (t, *J*=6.3 Hz, 2H), 1.96−1.89 (m, 2H), 1.88−1.80 (m, 2H), 1.61 (dd, *J*=15.4, 9.9 Hz, 4H), −2.91 (s, 2H); UV/Vis ($CHCl_3$): λ_{max}=269 nm (II band); 421 nm (Soret band); 519, 556, 594, and 650 nm (Q bands); fluorescence ($CHCl_3$): λ_{ex}=417 nm, λ_{em}=656 nm; MS (MALDI-TOF): *m/z* calcd for $C_{65}H_{50}N_4O_8^+$ 1014.36 $[M+H]^+$, found 1014.23.

Nickel(II)5-Hydroxy-2-phenyl-7-(2-(4-(10,15,20-tris(4-chlorophenyl)porphyrin-5-yl)phenoxy)ethoxy)-4*H*-chromen-4-one (5a) Yield 16%. ^{1}H NMR (500 MHz, $CDCl_3$): δ=12.75 (s, 1H), 8.79 (d, *J*=4.4 Hz, 2H), 8.72 (d, *J*=6.4 Hz, 6H), 7.93 (t, *J*=8.5 Hz, 9H), 7.89 (d, *J*=7.4 Hz, 2H), 7.67 (d, *J*=7.6 Hz, 6H), 7.52 (d, *J*=7.7 Hz, 3H), 7.24 (d, *J*=7.9 Hz, 2H), 6.68 (s, 1H), 6.60 (s, 1H), 6.48 (s, 1H), 4.43−4.36 (m, 4H); UV/Vis ($CHCl_3$): λ_{max}=269 nm (II band); 417 nm (Soret band); 529 nm (Q band); MS (MALDI-TOF): *m/z* calcd for $C_{61}H_{37}Cl_3N_4NiO_5^+$ 1068.12 $[M+H]^+$, found 1068.13.

Nickel(II)5-Hydroxy-2-phenyl-7-(3-(4-(10,15,20-tris(4-chlorophenyl)porphyrin-5-yl)phenoxy)propoxy)-4*H*-chromen-4-one (5b) Yield 15%. ^{1}H NMR (500 MHz, $CDCl_3$): δ=12.74 (s, 1H), 8.78 (d, *J*=4.4 Hz, 2H), 8.73−8.68 (m, 6H), 7.91 (t, *J*=8.5 Hz, 8H), 7.88 (d, *J*=7.4 Hz, 2H), 7.66 (d, *J*=7.6 Hz, 6H), 7.51 (d, *J*=7.7 Hz, 3H), 7.23 (d, *J*=7.9 Hz, 2H), 6.66 (s, 1H), 6.59 (s, 1H), 6.47 (s, 1H), 4.59−4.20 (m, 4H), 2.46 (s, 2H); UV/Vis ($CHCl_3$): λ_{max}=269 nm (II band); 417 nm (Soret band); 529 nm (Q band); MS (MALDI-TOF): *m/z* calcd for $C_{62}H_{39}Cl_3N_4NiO_5^+$ 1082.13 $[M+H]^+$, found 1082.14.

Nickel(II)5-Hydroxy-2-phenyl-7-(4-(4-(10,15,20-tris(4-chlorophenyl)porphyrin-5-yl)phenoxy)butoxy)-4*H*-chromen-4-one (5c) Yield 19%. ^{1}H NMR (500 MHz, $CDCl_3$): δ=12.75 (s, 1H), 8.80 (d, *J*=4.9 Hz, 2H), 8.73−8.69 (m, 6H), 7.91 (t, *J*=8.4 Hz, 8H), 7.86 (d, *J*=7.0 Hz, 2H), 7.66 (d, *J*=8.1 Hz, 6H), 7.52−7.45 (m, 3H), 7.21 (d, *J*=8.4 Hz, 2H), 6.65 (s, 1H), 6.54 (d, *J*=1.9 Hz, 1H), 6.43 (d, *J*=1.9 Hz, 1H), 4.29 (d, *J*=5.0 Hz, 2H), 4.20 (d, *J*=5.2 Hz, 2H), 2.15 (d, *J*=2.3 Hz, 4H); UV/Vis ($CHCl_3$): λ_{max}=269 nm (II band); 417 nm (Soret band); 529 nm (Q band); MS (MALDI-TOF): *m/z* calcd for $C_{63}H_{41}Cl_3N_4NiO_5^+$ 1096.15 $[M+H]^+$, found 1096.17.

Nickel(II)5-Hydroxy-2-phenyl-7-((5-(4-(10,15,20-tris(4-chlorophenyl)porphyrin-5-yl)phenoxy)pentyl)oxy)-4*H*-chromen-4-one (5d) Yield 18%. ^{1}H NMR (500 MHz, $CDCl_3$): δ=12.73 (s, 1H), 8.80 (d, *J*=4.9 Hz, 2H), 8.74−8.68 (m, 6H), 7.91 (dd, *J*=11.7, 8.4 Hz, 8H), 7.82 (d, *J*=7.2 Hz, 2H), 7.65 (d, *J*=8.1 Hz, 6H), 7.53−7.44 (m, 3H), 7.21 (d, *J*=8.4 Hz, 2H), 6.60 (s, 1H), 6.51 (d, *J*=2.1 Hz, 1H), 6.40 (d, *J*=2.1 Hz, 1H), 4.24 (t, *J*=6.2 Hz, 2H), 4.12 (t, *J*=6.3 Hz, 2H), 2.06−1.96 (m, 4H), 1.85−1.77 (m, 2H); UV/Vis ($CHCl_3$): λ_{max}=269 nm (II band); 417 nm (Soret band); 529 nm (Q band); MS (MALDI-TOF): *m/z* calcd for $C_{64}H_{43}Cl_3N_4NiO_5^+$ 1110.17 $[M+H]^+$, found 1110.18.

Nickel(II)5-Hydroxy-2-phenyl-7-((6-(4-(10,15,20-tris(4-chlorophenyl)porphyrin-5-yl)phenoxy)hexyl)oxy)-4*H*-chromen-4-one (5e) Yield 21%. ^{1}H NMR (500 MHz, $CDCl_3$): δ=12.72 (s, 1H), 8.80 (d, *J*=4.7 Hz, 2H), 8.74−8.68 (m, 6H), 7.91 (t, *J*=9.6 Hz, 8H), 7.80 (d, *J*=7.5 Hz, 2H), 7.65 (d, *J*=7.9 Hz, 6H), 7.52−7.41 (m, 3H), 7.21 (d, *J*=8.1 Hz, 2H), 6.58 (s, 1H), 6.48 (s, 1H), 6.39 (s, 1H), 4.21 (t, *J*=6.0 Hz, 2H), 4.08 (t, *J*=6.2 Hz, 2H), 2.03−1.96 (m, 2H), 1.96−1.89 (m, 2H), 1.74−1.62 (m, 4H); UV/Vis ($CHCl_3$): λ_{max}=269 nm (II band); 417 nm (Soret band); 529 nm (Q band); MS (MALDI-TOF): *m/z* calcd for $C_{65}H_{45}Cl_3N_4NiO_5^+$ 1124.18 $[M+H]^+$, found 1124.19.

Nickel(II)5-Hydroxy-2-phenyl-7-(2-(4-(10,15,20-tris(4-methoxyphenyl)porphyrin-5-yl)phenoxy)ethoxy)-4*H*-chromen-4-one (6a) Yield 15%. ^{1}H NMR (500 MHz, $CDCl_3$): δ=12.78 (s, 1H), 8.80−8.68 (m, 8H), 7.92 (q, *J*=8.3 Hz, 10H), 7.58−7.47 (m, 3H), 7.21 (d, *J*=8.5 Hz, 8H), 6.70 (s, 1H), 6.65 (d, *J*=2.0 Hz, 1H), 6.52 (d, *J*=2.0 Hz, 1H), 4.55 (d, *J*=10.1 Hz, 4H), 4.04 (s, 9H); UV/Vis ($CHCl_3$): λ_{max}=269 nm (II band); 419 nm (Soret band); 530 nm (Q band); MS (MALDI-TOF): *m/z* calcd for C64H46N4NiO8$^+$ 1056.27 $[M+H]^+$, found 1056.25.

Nickel(II)5-Hydroxy-2-phenyl-7-(3-(4-(10,15,20-tris(4-methoxyphenyl)porphyrin-5-yl)phenoxy)propoxy)-4*H*-chromen-4-one (6b) Yield 16%. ^{1}H NMR (500 MHz, $CDCl_3$) ^{1}H NMR (500 MHz, $CDCl_3$): δ=12.77 (s, 1H), 8.87 (d, *J*=5.3 Hz, 8H), 8.14 (d, *J*=7.2 Hz, 8H), 7.94−7.90 (m, 2H), 7.53 (d, *J*=6.9 Hz, 3H), 7.30 (d,

J=8.0 Hz, 8H), 6.71 (s, 1H), 6.66 (d, J=2.0 Hz, 1H), 6.52 (d, J=2.0 Hz, 1H), 4.46 (dt, J=13.1, 5.8 Hz, 4H), 4.11 (s, 9H), 2.54−2.49 (m, 2H); UV/Vis ($CHCl_3$): λ_{max}=269 nm (II band); 419 nm (Soret band); 530 nm (Q band); MS (MALDI-TOF): *m/z* calcd for $C_{65}H_{48}N_4NiO_8^+$ 1070.28 $[M+H]^+$, found 1070.25.

Nickel(II)5-Hydroxy-2-phenyl-7-(4-(4-(10,15,20-tris(4-methoxyphenyl)porphyrin-5-yl)phenoxy) butoxy)-4*H*-chromen-4-one (6c) Yield 17%. ^{1}H NMR (500 MHz, $CDCl_3$): δ=12.72 (s, 1H), 8.76 (s, 8H), 7.94−7.90 (m, 8H), 7.84 (d, J=6.6 Hz, 2H), 7.47 (t, J=7.6 Hz, 3H), 7.21 (d, J=8.3 Hz, 8H), 6.63 (s, 1H), 6.53 (s, 1H), 6.41 (s, 1H), 4.22 (t, J=6.1 Hz, 2H), 4.11 (t, J=6.3 Hz, 2H), 4.04 (s, 9H), 1.99 (d, J=6.9 Hz, 2H), 1.96−1.90 (m, 2H); UV/Vis ($CHCl_3$): λ_{max}=269 nm (II band); 419 nm (Soret band); 530 nm (Q band); MS (MALDI-TOF): m/z calcd for $C_{66}H_{50}N_4NiO_8^+$ 1084.30 $[M+H]^+$, found 1084.27.

Nickel(II)5-Hydroxy-2-phenyl-7-((5-(4-(10,15,20-tris(4-methoxyphenyl)porphyrin-5-yl)phenoxy)pentyl) oxy)-4*H*-chromen-4-one (6d) Yield 20%. ^{1}H NMR (500 MHz, $CDCl_3$): δ=12.73 (s, 1H), 8.76 (s, 8H), 7.92 (dd, J=5.9, 2.4 Hz, 8H), 7.85 (d, J=6.6 Hz, 2H), 7.52−7.44 (m, 3H), 7.21 (d, J=8.0 Hz, 8H), 6.63 (s, 1H), 6.54 (d, J=2.0 Hz, 1H), 6.42 (d, J=1.9 Hz, 1H), 4.24 (t, J=6.1 Hz, 2H), 4.14 (t, J=6.3 Hz, 2H), 4.04 (s, 9H), 2.07−1.98 (m, 4H), 1.82 (dd, J=15.0, 7.9 Hz, 2H); UV/Vis ($CHCl_3$): λ_{max}=269 nm (II band); 419 nm (Soret band); 530 nm (Q band); MS (MALDI-TOF): *m/z* calcd for $C_{67}H_{52}N_4NiO_8^+$ 1098.31 $[M+H]^+$, found 1098.28.

Nickel(II)5-Hydroxy-2-phenyl-7-((6-(4-(10,15,20-tris(4-methoxyphenyl)porphyrin-5-yl)phenoxy)hexyl) oxy)-4*H*-chromen-4-one (6e) Yield 21%. ^{1}H NMR (500 MHz, $CDCl_3$): δ=12.75 (d, J=2.0 Hz, 1H), 8.79 (d, J=2.1 Hz, 8H), 7.94 (dt, J=10.0, 3.5 Hz, 8H), 7.88−7.85 (m, 2H), 7.50 (td, J=7.4, 6.8, 3.2 Hz, 3H), 7.25−7.21 (m, 8H), 6.65 (s, 1H), 6.55 (d, J=2.3 Hz, 1H), 6.44 (d, J=2.2 Hz, 1H), 4.25 (t, J=6.4 Hz, 2H), 4.14 (d, J=6.4 Hz, 2H), 4.07 (s, 9H), 1.99 (dt, J=28.0, 6.9 Hz, 4H), 1.72 (d, J=14.1 Hz, 4H); UV/Vis ($CHCl_3$): λ_{max}=269 nm (II band); 419 nm (Soret band); 531 nm (Q band); MS (MALDI-TOF): *m/z* calcd for $C_{68}H_{54}N_4NiO_8^+$ 1112.33 $[M+H]^+$, found 1112.31.

Performance characterization

UV-Vis spectrometry. The test sample was dissolved in chloroform to prepare a working solution having a concentration of 10 μM, and the absorption spectra were scanned between 200 and 800 nm using a UV-Vis spectrophotometer.

Fluorescence spectrometry. The test compounds were accurately weighed using an analytical balance, and all the samples were dissolved in chloroform, and the sample was prepared as a test solution having a concentration of 10 μM. The samples were scanned using an F-7000 FL fluorescence spectrometer with a scanning range of 200–800 nm and an excitation wavelength of 418 nm.

$^1O_2$ detection. The test compounds were accurately weighed using an analytical balance and all the samples and DPBF were separately dissolved in chloroform. The sample was prepared as a test solution containing a sample (concentration: 10 μM) and DPBF (concentration: 100 μM). The samples were analyzed using an F-7000 FL fluorescence spectrometer. The excitation wavelength was set to 418 nm, the scanning speed was 2400 nm/min, the scanning range was 200–800 nm, and the scanning was performed at intervals of 1 min. The fluorescence changes of DPBF were recorded at 463 nm.

Biological activity detection

In vitro antitumor efficacy. The in vitro antitumor efficacy of the compounds was evaluated using the human tumor cells MGC-803 and HeLa cells in parallel with PDT. Each tested compound was dissolved in dimethyl sulfoxide (DMSO). The cells were plated in 96-well micro-titer plates at a density of 1×10^5 cells per well and incubated in a humidified atmosphere with 5% CO_2 at 37°C for 48 h. One of the experimental groups was removed after the first 4 h. The upper culture medium was carefully removed with a pipette and refilled with the drug-free culture fluid. Light was supplied by a 12 W LED purple lamp located 20 cm from the 96-well plate. Irradiation was continued for 10 min, after which the cells were placed in an incubator to continue the culture incubation. Test compounds of different concentrations (16, 32, 64, 128 μM) were added into triplicate wells and DMSO was used as the control. After 48 h, 20 mL of MTT solution (5 mg mL^{-1}) was added to each well, and incubation was continued for an additional 4 h. Formazan was dissolved in 150 mL of DMSO and added to the wells. The absorbance (optical density, OD) was monitored on a Wellscan MK-2 microplate reader (Lab-Systems) at 490 nm. The IC_{50} values were determined using the logit method. All experiments were performed three times.

Cell cycle analysis. The HeLa cells were plated in six-well plates (1×10^5 cells per well). After 24 h, the cells were incubated with different concentrations of compound **4a** (0, 20, 40, and 60 μM). One of the experimental groups was removed after the first 4 h. The upper culture medium was carefully removed with a pipette and refilled with the drug-free culture fluid. Light was supplied by a 12 W LED purple lamp (50 mW cm^{-2}, 380–460 nm), located 20 cm from the 96-well plate. After irradiation for 10 min, the cells were placed in an incubator to continue the culture incubation. After 24 h, the cells were washed twice with cold phosphate-buffered saline (PBS) and then re-suspended in cold PBS. Next, the cells were fixed and then stored in 70% cold ethanol for 12 h at 4°C. PI stain (500 mL) was added to the cells in each tube, and the cells were gently vortex mixed and then incubated for 30 min at 37°C in the dark. The cells were analyzed using flow cytometry within 24 h. All experiments were performed three times.

Cell apoptosis assay. The HeLa cells were plated in six-well plates (1×10^5 cells per well). After 24 h, the cells were

incubated with different concentrations of compound **4a** (0, 20, 40, and 60 μM). One of the experimental groups was removed after the first 4 h. The upper culture medium was carefully removed with a pipette and refilled with the drug-free culture fluid. Light was supplied by a 12 W LED purple lamp located 20 cm from the 96-well plate. After irradiation for 10 min, the cells were placed in an incubator to continue the culture incubation. After 24 h, the cells were washed twice with cold PBS and then re-suspended in binding buffer. Cells were transferred to a 5 mL culture tube, and then 5 mL of FITC Annexin V and 5 mL of PI were added to the cells. Next, the cells were gently vortex mixed and incubated for 15 min at 25°C in the dark. Subsequently, 400 mL of binding buffer was added to each tube. The cells were analyzed using flow cytometry within 1 h. All experiments were performed three times.

Acknowledgements

Ding Liu and Qizhi Zhang are contributed equally to this work and should be regarded as co-first authors.

Declaration of conflicting interests

The author(s) declared no potential conflicts of interest with respect to the research, authorship, and/or publication of this article.

Funding

The author(s) disclosed receipt of the following financial support for the research, authorship, and/or publication of this article: This work was supported by the Hunan Provincial Department of Education Key Project (grant no. 18A244), the Hunan Province University Students Research Learning and Innovative Experimental Project (grant no. S201910555017), and the Hunan Natural Science Foundation (grant no. 2018JJ2349).

ORCID iD

Yunmei Liu https://orcid.org/0000-0001-5931-3819

Supplemental material

Supplemental material for this article is available online.

References

1. Robertson CA, Evans DH and Abrahamse H. *J Photochem Photobiol B* 2009; 96: 1–8.
2. You Y, Liang X, Yin T, et al. *Theranostics* 2018; 8: 1665–1677.
3. Cheng M, Cui Y, Wang J, et al. *ACS Appl Mater Interfaces* 2019; 11: 13158.
4. Dosselli R, Tampieri C, Ruiz-González R, et al. *J Med Chem* 2013; 56: 1052–1063.
5. Park W, Cho S, Han J, et al. *Biomater Sci* 2017; 6: 79–90.
6. Kou J, Dou D and Yang L. *Oncotarget* 2017; 8: 81591–81603.
7. Feng X, Shi Y, Xie L, et al. *J Med Chem* 2018; 61: 7189–7201.
8. Elfar M and Pimstone N. *Cancer Res* 1986; 46: 4390–4394.
9. Brunner H, Arndt MR and Treittinger B. *Inorg Chim Acta* 2004; 357: 1649–1669.
10. Kubát P, Lang K and Anzenbacher P. *BBA: Gen Subjects* 2004; 1670: 40–48.
11. Polo L, Valduga G, Jori G, et al. *Int J Biochem Cell B* 2002; 34: 10–23.
12. Nakajima S, Takemura T and Sakata I. *Cancer Lett* 1995; 92: 113–118.
13. De Smidt P, Versluis A and van Berkel T. *Biochemistry* 1993; 32: 2916–2922.
14. Shibata Y, Matsumura A, Yoshida F, et al. *Cancer Lett* 2001; 166: 79–87.
15. Preihs C, Arambula JF, Magda D, et al. *Inorg Chem* 2013; 52: 12184–12192.
16. Cheng L, Jiang D, Kamkaew A, et al. *Adv Funct Mater* 2017; 27: 2928.
17. Hu X, Ogawa K, Kiwada T, et al. *J Inorg Biochem* 2017; 170: 1–7.
18. Lim W, Yang G, Phua S, et al. *ACS Appl Mater Interfaces* 2019; 11: 16391–16401.
19. Lotito S and Frei B. *J Biol Chem* 2006; 281: 37102–37110.
20. Shin EK, Kwon HS, Kim YH, et al. *Biochem Bioph Res Co* 2009; 381: 502–507.
21. Souza L, Antunes M, Filho C, et al. *Pharmacol Biochem Behav* 2015; 134: 22–30.
22. Freitas J and Gaspar L. *Eur J Pharm Sci* 2016; 89: 146–153.
23. Wang J, Qiu J, Dong JH, et al. *J Appl Microbiol* 2011; 111: 1551–1558.
24. Anand K, Jaabir M, Thomas P, et al. *Geriatr Gerontol Int* 2012; 12: 741–750.
25. Zhang T, Du J, Liu L, et al. *PLoS One* 2012; 7: e36652.
26. Dai T, Wang B, Lin S, et al. *Chin J Integr Med* 2017; 23: 370–375.
27. Xuan H, Zhang J, Wang Y, et al. *Bioorg Med Chem Lett* 2016; 26: 570–574.
28. Zheng X, Meng W, Xu Y, et al. *Bioorg Med Chem Lett* 2003; 13: 881–884.
29. Song X, Liu Y, Ma J, et al. *Med Chem Res* 2015; 24: 1789–1798.
30. Tang Q, Ji F, Guo J, et al. *Biomed Pharmacother* 2016; 82: 693–703.
31. Li H, Shi L, Li Q, et al. *Bioorgan Med Chem* 2009; 17: 6264–6269.
32. Valdez-Calderón A, González-Montiel S, Martínez-Otero D, et al. *J Mol Struct* 2016; 1110: 196–207.
33. Adler A, Longo F and Shergalis W. *J Am Chem Soc* 1964; 86: 3145–3149.
34. Huang S, Sun L and Ye Q. *Chem J Chinese U* 1983; 4: 381.
35. Zare-Dorabei R, Rahimi R, Koohi A, et al. *RSC Adv* 2015; 5: 93310–93317.
36. Zhao P, Liu M, Zheng M, et al. *J Nanosci Nanotechno* 2016; 16: 9843–9850.
37. Yang K, Liu Y, Feng X, et al. *Chem J Chinese U* 1991; 3: 400.
38. Abdolahzadeh S, Boyle NM, Hoogendijk ML, et al. *Dalton T* 2014; 43: 6322–6332.
39. Dai X, Wang Z, Gao L, et al. *New J Chem* 2014; 38: 3569–3578.
40. Jalde S, Chauhan A, Lee J, et al. *Eur J Med Chem* 2018; 147: 66–76.